Structural transformation mediated by *o*-, *m*-, and *p*-phthalates from two to three dimensions for manganese/phthalate/4,4′-bpy complexes (4,4′-bpy = 4,4′-bipyridine)

Chengbing Ma,[ad] Changneng Chen,[a] Qiutian Liu,*[a] Daizheng Liao,[b] Licun Li[b] and Licheng Sun[c]

[a] State Key Laboratory of Structural Chemistry, Fujian Institute of Research on the Structure of Matter, Chinese Academy of Sciences, Fuzhou, Fujian 350002, China.
E-mail: lqt@ms.fjirsm.ac.cn
[b] Department of Chemistry, Nankai University, Tainjin 300071, China
[c] State Key Laboratory of Fine Chemicals, Dalian University of Technology, Dalian, China
[d] Graduate School of the Chinese Academy of Sciences, Beijing, China

Three isomers of *o*-, *m*-, and *p*-phthalate are used to link together Mn centres, resulting in $[Mn(phth)(H_2O)_x]_n$ moieties (phth = phthalate dianion) with single-chain, double-chain and sheet structures, respectively, which predetermine the extended structures derived from the crosslinkage of 4,4′-bipyridine, and show the influence of isomerism of the phthalate on topological changes of the final polymers from two dimensional (2D) single-layer, double-layer to 3D network architectures. These structural changes in topology are correlated with the differences in the magnetic and optical properties of the polymers.

Introduction

Pronounced attention has currently been paid to the crystal engineering of 2D and 3D metal–ligand coordination polymers due to their fascinating network topologies and potential applications as functional materials.[1,2] Despite the upsurge in the construction of diverse architectures, the control of dimensionality is still a major challenge in this field[3] due to the fact that the resultant structural framework is frequently influenced by various factors such as medium, temperature, metal–ligand ratio, template and counter-ion.[4] In a spontaneous assembly process, the structural information stored in the organic ligand is read by the metal ion through its coordination geometry from the programmed system.[5] By the judicious choice of the organic spacer and the central metal, it is possible to elaborate a specific architecture, and even to create expected properties related to the architecture. Scheme 1 illustrates the controlled formation of the topological framework, which predictably varies from 2D (single-layer, double-layer, *etc.*) to 3D for the given octahedral metal. In this process, primary ligand

L^1 completes the coordination equatorial plane, forming 1D chain or 2D layer structures, while *exo*-bidentate axial ligand L^2 as a secondary spacer leads to the final architectures with higher dimensionality. Three manganese(II) polymers are reported in this work, exhibiting systematic structural variation from 2D single-layer to 2D double-layer to 3D network. Their magnetic behaviors and fluorescence are also presented.

Synthesis

We have reported a double-chain structure of a Mn complex $[Mn(m\text{-}phth)(C_5H_5N)_2]_n$[6] with *m*-phthalate as the primary ligand L^1 for the first time by using monodentate pyridine as the secondary axial ligand (L^2) as shown in Scheme 2. It seems to be predictable that *exo*-bidentate 4,4′-bipyridine (4,4′-bpy) should lead to the 2D double-layer structure if it is used as L^2 instead of monodentate pyridine. Three phthalate isomers are picked out as the primary ligand, in view of their versatile bonding modes with metal ion(s), together with 4,4′-bpy as the
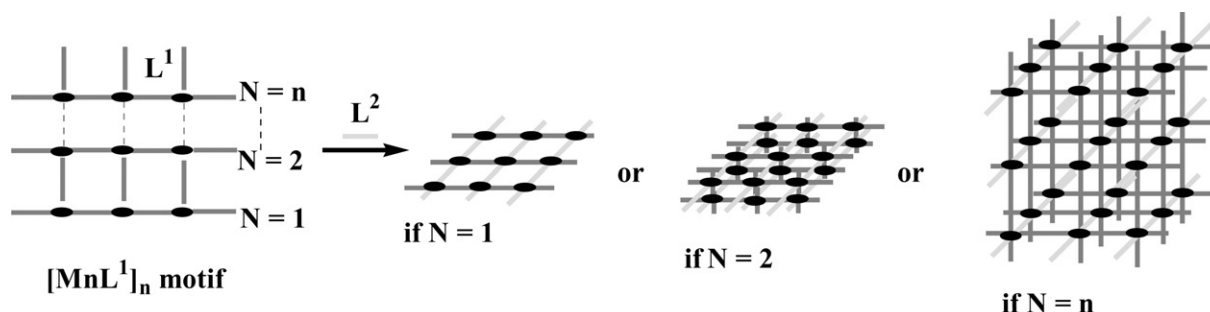
Scheme 1 Schematic representation of assembly for possible architectures. Octahedral metal (black ellipse) is coordinated by primary ligands L^1 in the equatorial plane to form single-chain ($N = 1$), double-chain ($N = 2$) and sheet motifs ($N = n$). Secondary organic spacers L^2 enter axial positions, forming 2D single-layer, 2D double-layer, and 3D network structures. The capital letter N stands for the number of layers in the $[MnL^1]_n$ motif.

DOI: 10.1039/b301076g
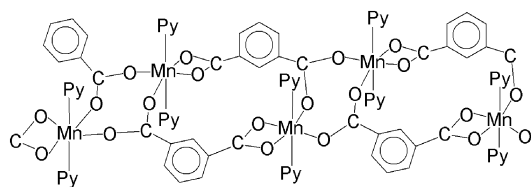
Scheme 2 A double chain structure of $[Mn(m\text{-phth})(py)_2]_n$.

secondary spacer, to observe the influence of isomerism of the phthalate on the topology of the synthesized Mn polymers. Hydrothermal reactions of $MnCO_3$ with *o*, *m*, or *p*-phthalic acid isomers and 4,4′-bpy were performed in water–ethanol at 160 °C, affording $[Mn(o\text{-phth})(4,4'\text{-bpy})(H_2O)_2]_n$ (**1**), $[Mn(m\text{-phth})(4,4'\text{-bpy})]_n$ (**2**) and $[Mn(p\text{-phth})(4,4'\text{-bpy})]_n$ (**3**), respectively, in moderate yields.

Structure and dimensionality

The three compounds are constructed from $[Mn(phth)(H_2O)_x]_n$ (L = *o*-phth, *x* = 2 and L = *m*- or *p*-phth, *x* = 0) motifs linking 4,4′-bpy spacers. The motif of **1** has a single-chain structure (Fig. 1a), in which two carboxyls of the *o*-phth ligand coordinate monodentately to two Mn centers forming a Mn–phth–Mn linkage and two water molecules are located at opposite sides of the equatorial plane. This motif is different from that found in $[Mn(o\text{-phth})(phen)(H_2O)_2]_n \cdot H_2O$,[7] in which *o*-phth employs one carboxyl bridging Mn atoms to form a chain structure with another carboxyl free. $[Mn(m\text{-phth})]_n$ contains a parallel double-chain with respect to the Mn atoms, in which the one carboxyl of the *m*-phth chelates to a Mn and the other bridges between two Mn atoms (Fig. 1b). A quite different example was found to be $[Zn_4(m\text{-phth})_4(\mu_4\text{-O})(bpy)_4]_n$,[8] in which the Zn_4O cores are bridged by bis-monodentate and bis-bidentate *m*-phth ligands into 1D ladder-like $[Zn_4O(m\text{-phth})_3]$ chains. $[Mn(p\text{-phth})]_n$ has a parallelogram-grid sheet structure. Every *p*-phth ligand in μ_4-bridging mode links two pairs of adjacent Mn atoms, resulting in 1D linear chains with Mn···Mn separation of 4.196(2) Å, which are further inter-linked through *p*-phth ligands in bis-bidentate chelating mode to fabricate a 2D sheet (Fig. 1c). A similar coordination mode of *p*-phth to that in **3** has been found in $[Co(p\text{-phth})(bpy)]_n$.[9]

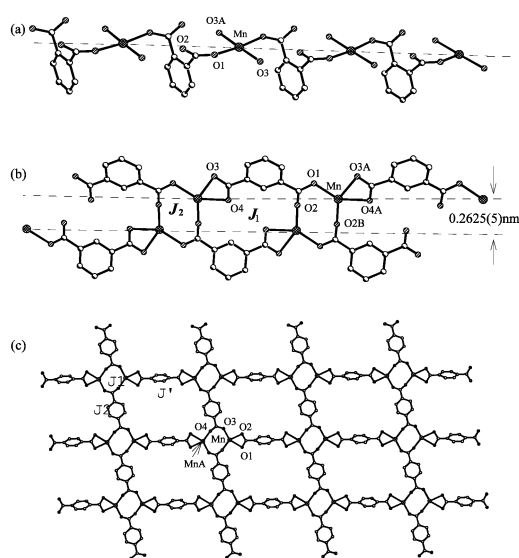**Fig. 1** Structures of three motifs in **1**, **2** and **3**. (a) 1D single-chain of $Mn(o\text{-phth})(H_2O)_2$, (b) 1D double-chain of $Mn(m\text{-phth})$, and (c) 2D sheet of $Mn(p\text{-phth})$. Selected atoms are labeled with the Mn chains dotted and 4,4′-bpy omitted. Possible magnetic interaction routes are indicated.
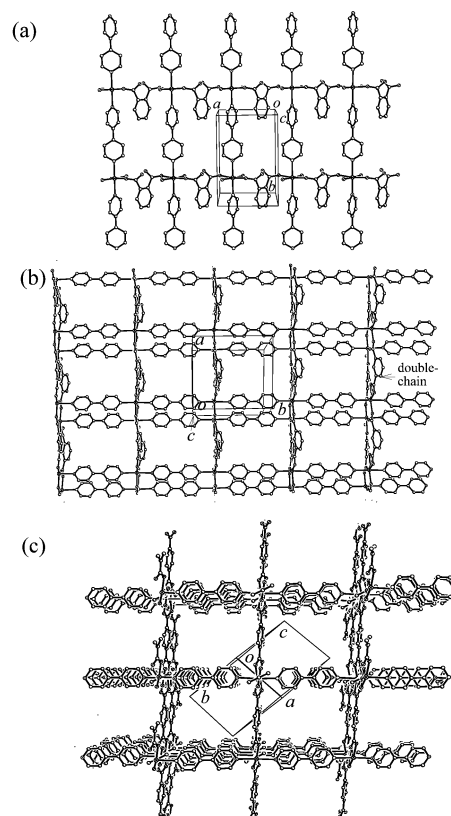

Fig. 2 Perspective views of the frameworks pillared by 4,4′-bpy for three manganese polymers: (a) 2D single-layer, (b) 2D double-layer, and (c) 3D network in **1**, **2** and **3**, respectively.

The three motifs mentioned above are further linked by bidentate 4,4′-bpy along the axial positions of the Mn octahedron, creating three different architectures: a 2D wavy single-layer of **1** having rectangular grids with dimensions of $7.704(1) \times 11.586(1)$ Å (Fig. 2a), a 2D parallel double-layer of **2** with an interlayer separation of *ca.* 2.625(5) Å (Fig. 2b) and a 3D two-fold interpenetrating network of **3** containing 1D channels with dimensions of $11.598(1) \times 10.929(1)$ Å (Fig. 2c). Selected bond distances and angles are listed in Table 1. Unlike **1** and **2**, no guest molecules are encapsulated in **3** due to the large pores which are actually filled by interpenetration of a second network. The complicated coordination modes of *o*- and *p*-phth ligands in **1** and **3** are rarely found, though similar structures to **1** and **3** have occurred in three Co and Cd complexes.[9,10] As mentioned previously, the double-chain motif of the *m*-phth ligand has recently been reported,[6] which leads to complex **2** with a novel double-layer structure pillared by 4,4′-bpy. A few metal complexes with bilayer[11] or trilayer[12] structures have been reported.

A notable structural feature in the three polymers is the occurrence of $[Mn(phth)(H_2O)_x]_n$ subunits, which predetermine the extended orientations of the final structure. It is logical that the smallest separation of carboxyls in *o*-phth compared to that in *m*- and *p*-isomers results in crowding of the groups, which is favorable for the monodentate coordination of both the *o*-COO groups to Mn ions, forming a $[Mn(o\text{-phth})(H_2O)_2]_n$ single-chain structure. It is also noted that, with the decrease of the steric crowding of the two carboxylic groups, the dihedral angle between them becomes smaller from 54.4(5)° in **1** to 12.8(5)° in **2**. A similar variation of the dihedral angle between the carboxylic group and the neighbouring benzene ring is also observed from 120.6(1)° in **1** to 11.3(2)° in **2**. In complex **3**, all the carboxyl groups in the same layer are strictly coplanar, and the coplanarity can extend to include all the Mn sites and the μ_4-*p*-phth ligands. Obviously, it is the isomeric phthalates that play a vital role in the controlled

Table 1 Selected bond distances (Å) and angles (°) of **1**, **2** and **3**

1

Mn–O1	2.196(2)	Mn–O3	2.203(2)
Mn–N1	2.252(4)	Mn–N2B	2.268(4)
O1–Mn–O1A	172.73(12)	O1–Mn–O3A	92.91(9)
O1–Mn–O3	86.99(8)	O3–Mn–O3A	178.45(12)
O1–Mn–N1	93.64(6)	O3–Mn–N1	90.77(6)
O1–Mn–N2B	86.36(6)	O3–Mn–N2B	89.23(6)
N1–Mn–N2B	180.00(1)		

2

Mn–O1	2.142(3)	Mn–O2B	2.101(3)
Mn–O4A	2.227(3)	Mn–N2C	2.232(4)
Mn–N1	2.266(3)	Mn–O3A	2.302(3)
O2B–Mn–O1	124.22(11)	O2B–Mn–O4A	90.26(12)
O1–Mn–O4A	145.46(11)	O2B–Mn–N2C	88.43(12)
O1–Mn–N2C	90.68(11)	O4A–Mn–N2C	92.35(12)
O2B–Mn–N1	88.20(12)	O1–Mn–N1	88.36(11)
O4A–Mn–N1	91.12(12)	N2C–Mn–N1	175.17(12)
O2B–Mn–O3A	147.43(11)	O1–Mn–O3A	88.22(10)
O4A–Mn–O3A	57.25(10)	N2C–Mn–O3A	94.68(13)
N1–Mn–O3A	90.02(13)		

3

Mn–O4A	2.065(3)	Mn–O3	2.106(3)
Mn–O2	2.193(3)	Mn–N2B	2.266(4)
Mn–N1	2.278(4)	Mn–O1	2.356(3)
O4A–Mn–O3	116.31(13)	O4A–Mn–O2	151.01(13)
O3–Mn–O2	91.57(12)	O4A–Mn–N2B	90.89(13)
O3–Mn–N2B	94.22(13)	O2–Mn–N2	94.97(14)
O4A–Mn–N1	88.18(13)	O3–Mn–N1	89.80(13)
O2–Mn–N1	83.94(14)	N2B–Mn–N1	175.86(13)
O4A–Mn–O1	95.09(12)	O3–Mn–O1	148.54(13)
O2–Mn–O1	57.07(11)	N2B–Mn–O1	86.79(13)
N1–Mn–O1	89.28(14)		

formation of final architectures with structural systematic variation by means of specific location and orientation of two carboxyl groups.

Magnetic properties and emission spectra

Experimental effective magnetic moments as functions of temperature for **1**, **2** and **3** are shown in Fig. 3. Considering a separation between the Mn(II) centers bridged by 4,4′-bpy which is too long to transfer the magnetic interactions, two models based on a uniform $[Mn(\mu\text{-}o\text{-phth})]_n$ chain[13] (Fig. 1a) and alternating chains[14] consisting of $Mn_2(\mu\text{-}OCO)_2$ and $Mn_2(\mu_3\text{-}m\text{-phth})_2$ moieties (Fig. 1b) were adopted for **1** and **2**, respectively. Two possible magnetic exchange interactions were contained in the models: a long pathway (J_1) through
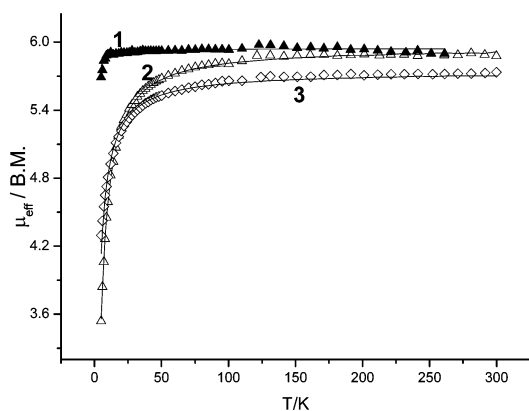

Fig. 3 Temperature dependence of effective magnetic moments (μ_{eff}) for complexes **1**, **2** and **3**. The solid lines represent the calculated values.

the phthalate ligand and a short μ-OCO way (J_2). Eqns. 1 and 2 were used to fit the magnetic data of **1** and **2**, respectively.

$$\chi_1 = \left(\frac{Ng^2\mu_B^2}{kT}\right)[A + Bx^2][1 + Cx + Dx^3]^{-1}$$

$$A = 2.9167, \quad B = 208.04, \quad C = 15.543,$$

$$D = 2707.2, \quad x = |J_l|/kT \tag{1}$$

$$\chi_2 = \frac{Ng'^2\mu_B^2}{3kT}\left(\frac{1 + u_1 + u_2 + u_1u_2}{1 - u_1u_2}\right)$$

$$u_1 = \mathrm{Coth}\left(\frac{J'_1}{kT}\right) - \frac{kT}{J'_1} \qquad u_2 = \mathrm{Coth}\left(\frac{J'_2}{kT}\right) - \frac{kT}{J'_2}$$

$$J'_i = J_i S(S + 1) \quad (i = 1, 2); \quad g' = g[S(S + 1)]^{1/2} \tag{2}$$

The best fitting parameters were found to be $J_1 = -0.01$ cm^{-1}, $g = 2.01$, and $R = 3.89 \times 10^{-4}$ for **1**, $J_1 = -0.08$ cm^{-1}, $J_2 = -1.05$ cm^{-1}, $g = 2.01$, and $R = 5.57 \times 10^{-5}$ for **2**.

For **3**, it was first treated as a dinuclear manganese unit $Mn_2(\mu\text{-}OCO)_2$ with the interaction being J_1.

$$\hat{H} = -J_1\hat{S}_1 \cdot \hat{S}_2 \tag{2}$$

These dinuclear units can be seen as entities with effective classical spin S_{bi} which link each other through planar μ_4-p-phth bridges to form a 1D chain with the magnetic exchange constant (J_2) between the Mn ions of neighboring entities. This 1D S_{bi} chain can be treated according to eqn. 3 to obtain the susceptibility values.

$$\chi_{chain} = [Ng^2\beta^2 S_{bi}(S_{bi} + 1)/3kT]\left(\frac{1 + u}{1 - u}\right)$$

$$u = \mathrm{Coth}\left[\frac{J_2 S_{bi}(S_{bi} + 1)}{kT}\right] - \frac{kT}{J_2 S_{bi}(S_{bi} + 1)} \tag{3}$$

Then a molecular field approximation[15] (eqn. 4) was used to modify the interchain interaction (zJ') through the chelating p-phth bridge (Fig. 1c), giving the final susceptibilities of the system. The z value is the number of nearest magnetic species around a given magnetic site in the crystal lattice.

$$\chi_M = \frac{\chi_{chain}}{1 - (zJ'/Ng^2\beta^2)\chi_{chain}} \tag{4}$$

The best fitting parameters were found to be $J_1 = -0.44$ cm^{-1}, $J_2 = -0.155$ cm^{-1}, $zJ' = -0.062$ cm^{-1}, $g = 1.98$, and $R = 9.27 \times 10^{-4}$ for **3**.

All the magnetic interactions in the three complexes are weak antiferromagnetic coupling interactions. It is noted that the magnetic interactions through the short μ-OCO pathway are obviously larger than that through the long pathway including the benzene ring of the phthlates. The difference in the magnitude of the magnetic coupling interactions found for the three complexes can be explained in terms of the bridging modes and the overlap of d–p magnetic orbitals. As expected on the basis of the respective geometries, an efficient overlap between the 3d magnetic orbital of the Mn^{2+} center and the 2p magnetic orbital of the carboxyl oxygen atom would lead to antiferromagnetic interactions. As mentioned previously the three complexes exhibit evidently different coplanarity between the caboxylic group and neighbouring benzene ring in the order p- > m- > o- for the isomers. Consequently, the magnitude of the magnetic interactions *via* the long pathway becomes **3** > **2** > **1**.

The emission spectra in the solid state at room temperature are shown in Fig. 4 for **1** and **2** and Fig. 5 for **3**. There are significant differences of the emission maxima for the three complexes. The photoluminescence of **1** exhibits an intense emission maximum at 610 nm ($\lambda_{exc} = 432$ nm), while **2** has complicated spectral features with two stronger emission

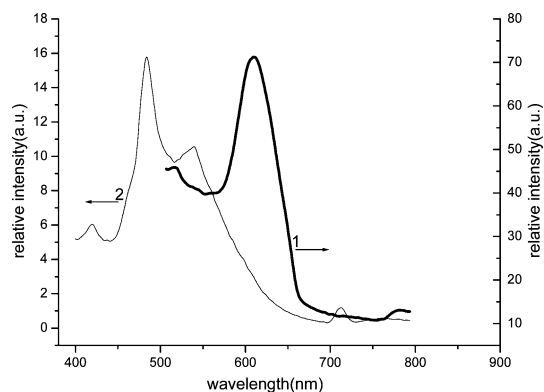**Fig. 4** Solid state emission spectra of **1** and **2** at room temperature.
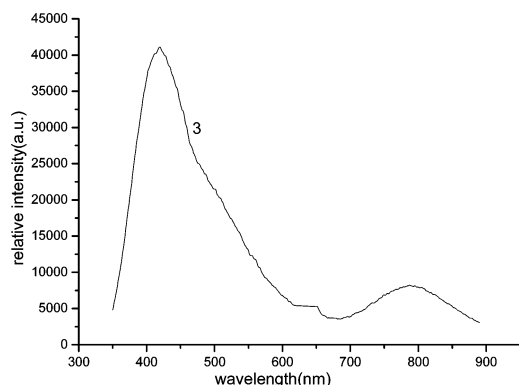

Fig. 5 Solid state emission spectrum of **3** at room temperature.

maxima at 485 nm and 538 nm, as well as two weaker ones at 419 nm and 712 nm (λ_{exc} = 350 nm). **3** exhibits one strong emission maximum at 420 nm and two weak peaks at 650 nm and 790 nm (λ_{exc} = 320 nm). The complicated mixed-ligand system and the lack of available information on photoluminescence for the Mn(II) complex make assignment of the observed emissions difficult; however, these variations, especially for the most intense emission, seem to be correlated to the introduction of three phthalate isomers resulting in corresponding structural variations. Further work is in progress.

In conclusion, we have created three manganese(II) polymers exhibiting a systematic variation of topologies by the utilization of isomeric ligands, and representing a preliminary example of realizing structural transformation from single-layer to double-layer to 3D network. Though approaches of controlling the dimensionality of the coordination polymers are developing, only a few series of isomeric organic ligands, to our knowledge, have been utilized to study for this purpose. The isomeric phthalates not only give rise to systematic variation of structural topologies in the presence of 4,4′-bpy for the given Mn(II) center, but also alter the magnetic and photoluminescent properties, providing crystal engineering with a potential tool for tuning the crystalline solid architecture and exploring desirable properties.

Experimental

Synthesis

1 · 2*n*H₂O. In a typical synthesis, 0.23 g (2 mmol) of $MnCO_3$, 0.34 g (2 mmol) of *o*-phthalic acid and 0.31 g (2 mmol) of 4,4′-bipyridine and 15 mL of water–ethanol (v/v, 1:1) were sealed in a 25 ml stainless-steel reactor with a teflon liner. The reactor was heated to 160 °C during 4 hours, and kept at this temperature for 4 days. This gave 0.48 g of light yellow block-like crystals of **1**·2H₂O in 54% yield (based on

Mn). Anal. Calcd. for $C_{18}H_{20}MnN_2O_8$: C, 48.33; H, 4.51; N, 6.26; Mn, 12.28. Found: C, 48.37; H, 4.49; N, 6.32; Mn, 12.33%. IR (KBr pellet, cm⁻¹): ν = 3458(s), 3178(br), 1635(m), 1606(s), 1560(s), 1535(w), 1485(m), 1443(m), 1406(s), 1317(w), 1217(w), 1082(w), 1065(w), 1049(w), 1012(m), 947(w), 839(m), 800(w), 764(s), 737(w), 698(w), 671(w), 656(w), 633(s), 567(w), 530(m), 513(w), 444(w).

2 · 0.75*n*H₂O · 0.25*n*C₂H₅OH. The preceding procedure was utilized with the use of *m*-phthalic acid instead. Yellow rhombic crystals (0.62 g) were obtained in 77% yield (based on Mn). Anal. Calcd. for $C_{18.5}H_{15}MnN_2O_5$: C, 55.51; H, 3.78; N, 7.00; Mn, 13.73. Found: C, 55.55; H, 3.83; N, 6.98; Mn, 13.79%. IR (KBr pellet, cm⁻¹): ν = 3430(br), 3095(w), 3059(m), 2924(w), 2848(w), 1682(s), 1605(s), 1568(s), 1547(s), 1479(m), 1446(s), 1394(s), 1327(w), 1277(w), 1259(w), 1221(m), 1157(w), 1103(m), 1070(s), 1045(s), 1007(s), 960(w), 937(w), 914(m), 881(w), 833(m), 812(s), 741(s), 721(s), 660(m), 629(s), 573(m), 509(w), 428(m).

3. The preceding procedure was utilized with the use of *p*-phthalic acid instead. 0.28 g of light yellow prismatic crystals were collected in 37% yield (based on Mn). Anal. Calcd. for $C_{18}H_{12}MnN_2O_4$: C, 57.62; H, 3.22; N, 7.47; Mn, 14.64. Found: C, 57.58; H, 3.27; N, 7.45; Mn, 14.71%. IR (KBr pellet, cm⁻¹): ν = 3110(w), 1657(m), 1610(s), 1556(s), 1493(w), 1417(s), 1369(s), 1223(m), 1142(w), 1068(s), 1045(w), 1012(m), 891(w), 858(w), 839(w), 812(s), 793(w), 752(s), 729(w), 656(w), 633(s), 573(w), 501(m), 478(m), 442(w).

X-Ray crystallography

Single crystals of the three complexes were coated with epoxy resin and mounted on a glass fiber and scanned on a Siemens Smart CCD diffractometer with Mo Kα radiation (λ = 0.71073 Å) at 293 K using the ω–2θ scan mode. The structures were solved by direct methods and refined by full-matrix least squares on (F^2) by using the SHELXTL97 program.[16] The metal ions were first located, while other non-hydrogen atoms were found in subsequent difference Fourier syntheses. All the non-hydrogen atoms were refined anisotropically except for the O8 atom of complex **2**, which is in solvate EtOH and has an occupancy factor of 0.25 in its position which was refined

Table 2 Crystallographic data for **1**·2*n*H₂O, **2**·0.75*n*H₂O·0.25*n*-C₂H₅OH and **3**

Compound	**1**·2*n*H₂O	**2**·0.75*n*H₂O·0.25*n*C₂H₅OH	**3**
Formula	$C_{18}H_{20}MnN_2O_8$	$C_{18.5}H_{15}MnN_2O_5$	$C_{18}H_{12}MnN_2O_4$
f.w.	447.30	400.26	375.24
Space group	$P2/n$	$P2/c$	$P\bar{1}$
a/Å	7.7038(9)	10.116(2)	9.3349(7)
b/Å	11.5864(13)	11.562(2)	10.3142(8)
c/Å	10.7693(12)	16.084(3)	11.4065(8)
α/°	90.00	90.00	92.023(1)
β/°	92.691(2)	102.99(3)	112.864(1)
γ/°	90.00	90.00	116.479(2)
V/Å³	960.20(19)	1833.0(6)	876.36(11)
Z	2	4	2
d_{calc}/g cm⁻³	1.547	1.450	1.422
μ/mm⁻¹	0.737	0.752	0.777
T/K	293	293	293
$2\theta_{max}$/°	25.02	27.52	25.05
No. unique reflections	1694 (R_{int} = 0.0317)	3990 (R_{int} = 0.0476)	3066 (R_{int} = 0.0272)
Reflections used ($I > 2\sigma(I)$)	1292	2799	2313
$R_1{}^a$	0.0430	0.0631	0.0568
$R_w{}^b$	0.1008	0.1783	0.1379

^{a} $R = \Sigma||F_o| - |F_c||/\Sigma|F_o|$. ^{b} $R_w = [\Sigma w(|F_o| - |F_c|)^2/\Sigma wF_o^2]^{1/2}$.

isotropically. Hydrogen atoms were located by geometric calculation, but their positions and thermal parameters were fixed during the structure refinement. It is necessary to indicate that complex **2** contains solvate H_2O and EtOH in its lattice, which were found to form only 0.75 and 0.25 molecules in various positions. The crystallographic data of the three complexes are listed in Table 2.

CCDC reference numbers: 190374–190376 for **1**–**3**. See http://www.rsc.org/suppdata/nj/b3/b301076g/ for crystallographic data in CIF or other electronic format.

Acknowledgements

References

1 (*a*) R. Robson, B. F. Abrahams, S. R. Batten, R. W. Gable, B. F. Hoskins and J. Liu, *Supramolecular Architecture*, ACS, Washington, DC, 1992; (*b*) S. R. Batten and R. Robson, *Angew. Chem., Int. Ed.*, 1998, **37**, 1460–1494; (*c*) M. J. Zaworotko, *Chem. Commun.*, 2001, 1–9; (*d*) P. J. Hagrman and J. Zubieta, *Angew. Chem., Int. Ed.*, 1999, **38**, 2638–2384; (*e*) O. M. Yaghi, H. Li, C. Davis, D. Richardson and T. L. Groy, *Acc. Chem. Res.*, 1998, **31**, 474–484; (*f*) M. Munakata, L. Wu and T. K. Sowa, *Adv. Inorg. Chem.*, 1999, **46**, 173–197; (*g*) A. J. Blake, N. R. Champness, P. Hubberstey, W.-S. Li, M. A. Withersby and M. Schröder, *Coord. Chem. Rev.*, 1999, **183**, 117–138; (*h*) J. M. Lehn, *Angew. Chem., Int. Ed.*, 1988, **27**, 89–112.

2 (*a*) O. Kahn and C. Martinez, *Science*, 1998, **279**, 44–48; (*b*) O. M. Yaghi, G. M. Li and H. L. Li, *Nature*, 1995, **378**, 703–705; (*c*) M. Fujita, Y. J. Kwon, S. Washizu and K. Ogura, *J. Am. Chem. Soc.*, 1994, **116**, 1151–1152; (*d*) S. Subramanian and M. J. Zaworotko, *Angew. Chem., Int. Ed. Engl.*, 1995, **34**, 2127–2129; (*e*) J. S. Miller and A. J. Spstein, *Chem. Commun.*, 1998, 1319–1320; (*f*) M. S. E. Fallah, E. Rentschler, A. Caneschi, R. Sessoli and D. Gatteschi, *Angew. Chem., Int. Ed. Engl.*, 1996, **35**, 1947–1948.

3 S. S.-Y. Chui, S. M.-F. Lo, J. P. H. Charmant, A. G. Orpen and I. D. Williams, *Science*, 1999, **283**, 1148–1150.

4 (*a*) Y. Tokunaga, D. M. Rudkevich and J. Jr. Rebek, *Angew. Chem., Int. Ed. Engl.*, 1997, **36**, 2656–2659; (*b*) M. A. Withersby, A. J. Blake, N. R. Champness, P. Hubberstey, W. Li and M. Schröder, *Angew. Chem., Int. Ed. Engl.*, 1997, **36**, 2327–2329; (*c*) O. M. Yaghi and H. Li, *J. Am. Chem. Soc.*, 1995, **117**, 10 401–10 402; (*d*) P. Losier and M. J. Zaworotko, *Angew. Chem., Int. Ed. Engl.*, 1996, **35**, 2779–2781 and references therein; (*e*) D. M. J. Dobe, C. H. Benison, A. J. Blake, D. Fenske, M. S. Jackson, R. D. Kay, W. Li and M. Schröder, *Angew. Chem., Int. Ed.*, 1999, **38**, 1915–1918.

5 J. M. Lehn, *Supramolecular Chemistry-Concepts and Perspectives*, VCH, Weinheim, 1995.

6 M. Eddaoudi, D. B. Moler, H. Li, B. Chen, T. M. Reineke, M. O. Keeffe and O. M. Yaghi, *Acc. Chem. Res.*, 2001, **34**, 319–330.

7 Y. Zhang, J. Li, M. Zhu, Q. Wang and X. Wu, *Chem. Lett.*, 1998, 1051–1052.

8 J. Tao, M.-L. Tong, J.-X. Shi, X.-M. Chen and S. W. Ng, *Chem. Commun.*, 2000, 2043–2044.

9 J. Tao, M.-L. Tong and X.-M. Chen, *J. Chem. Soc., Dalton Trans.*, 2000, 3669–3674.

10 E. Suresh, K. Boopalan, R. V. Jasra and M. M. Bhadbhade, *Inorg. Chem.*, 2001, **40**, 4078–4080.

11 (*a*) S. Kitagawa and M. Kondo, *Bull. Chem. Soc. Jpn.*, 1998, **71**, 1739–1753; (*b*) C. J. Kepert and M. J. Rosseinsky, *Chem. Commun.*, 1999, 375–376; (*c*) A. Rujiwatra, C. J. Kepert and M. J. Rosseinsky, *Chem. Commun.*, 1999, 2307–2308; (*d*) K. N. Power, T. L. Hennigar and M. J. Zaworotko, *New J. Chem.*, 1998, **22**, 177–181; (*e*) J. Dai, X. Wu, Z. Fu, C. Cui, S. Hui, W. Du, L. Wu, H. Zhang and R. Sun, *Inorg. Chem.*, 2002, **41**, 1391–1396.

12 J. Y. Lu and A. M. Babb, *Inorg. Chem.*, 2001, **40**, 3261–3262.

13 W. Hiller, J. Strähle, A. Datz, M. Hanack, W. E. Hatfield, L. W. ter Haar and P. Gütlich, *J. Am. Chem. Soc.*, 1984, **106**, 329–335.

14 R. Cortés, M. Drillon, X. Solans, L. Lezama and T. Rojo, *Inorg. Chem.*, 1997, **36**, 677–683.

15 (*a*) C. J. O'Connor, *Prog. Inorg. Chem.*, 1982, **29**, 203; (*b*) M. Handa, Y. Sayama, M. Mikuriya, R. Nukada, I. Hiromitsu and K. Kasuga, *Bull. Chem. Soc. Jpn.*, 1998, **71**, 119; (*c*) H.-Y. Shen, W.-M. Bu, E.-Q. Gao, D.-Z. Liao, Z.-H. Jiang, S.-P. Yan and G.-L. Wang, *Inorg. Chem.*, 2000, **39**, 396.

16 G. M. Sheldrick, SHELXTL97, Program for the Refinement of Crystal Structures, University of Göttingen, Germany, 1997.